TM-2260

# SOME STABILITY ISSUES OF THE FERMILAB DAMPING RING

K.Y. Ng

*Fermi National Accelerator Laboratory,* P.O. Box 500, Batavia, IL 60510*

(July, 2004)

**Abstract**

From a special injection scheme, the TESLA 17 km damping ring can be reduced in size to about 6 km. Some stability issues of this Fermilab design are discussed. This design will be safe against single-bunch coupled-mode instabilities, both longitudinal and transverse. Coupled-bunch instabilities will be mild. Effects of electron clouds as well as trapped ions are also discussed.

Based on a talk given at
Linear Collider Workshop
Victoria, BC, Canada
July 27-30, 2004

*Operated by the Universities Research Association, Inc., under contract with the U.S. Department of Energy.

# 1 FERMILAB DESIGN

A 1 ms pulse of the TESLA design contains 2820 bunches with 337 ns separation,[†] and is compressed to 20 ns separation on entering the dog-bone damping ring, which has a circumference of 17 km. The Fermilab design injects the 2820 TESLA bunches into 60 trains containing 47 bunches each. The bunch separation is $\tau_{\text{sep}} = 6$ ns and the train separation is 340 ns for the first 59 trains and $340 - 6 = 334$ ns for the last train. Thus the train gap is $334 - 6 \times 46 = 64$ ns except for the last one which is 6 ns shorter. Some properties of the Fermilab damping ring are listed in Table I.

# 2 IMPEDANCE OF VACUUM CHAMBER

## 2.1 Space Charge

The Fermilab damping ring is designed for the beam energy $E = 5.066$ GeV with a ring circumference $C = 2\pi R = 6113.97$ m. The designed normalized rms beam emittances are $\epsilon_{xN} = 4.66 \times 10^{-6}$ $\pi$m and $\epsilon_{yN} = 2.00 \times 10^{-8}$ $\pi$m, with betatron tunes $\nu_x = 59.28$ and $\nu_y = 45.10$. The mean betatron functions are therefore $\bar{\beta}_x = 16.41$ m and $\bar{\beta}_y = 21.57$ m. The rms vertical beam radius is

$$\sigma_y = \sqrt{\frac{\bar{\beta}_y \epsilon_{yN}}{\gamma}} = 6.60\ \mu\text{m}\ , \tag{2.1}$$

where $E = \gamma mc^2$ is the electron energy, $m$ its rest mass, and $c$ the velocity of light. The horizontal rms dispersion function is $\eta_{\text{rms}} = 0.213$ m and the rms energy spread $\sigma_E = 0.001513$. Since dispersion function of the lattice and energy offset of a particle in the beam are statistically independent, the rms horizontal beam radius is therefore

$$\sigma_x = \sqrt{\frac{\bar{\beta}_x \epsilon_{xN}}{\gamma} + (\eta_{\text{rms}}\sigma_E)^2} = 334\ \mu\text{m}\ , \tag{2.2}$$

Notice that the horizontal emittance contributes only 87.9 $\mu$m to the beam size whereas the dispersion contributes 322.5 $\mu$m. Thus the average horizontal beam size is dominated by dispersion. The TESLA dog-bone ring, on the other hand, is quite different. The arcs

[†]This 337-ns bunch separation is modified to 340 ns for use with the Fermilab designed damping ring.

Table I: Some properties of the Fermilab damping ring.

| | |
|---|---|
| **Lattice** | |
| Circumference $C$ (m) | 6113.967 |
| Energy $E$ (GeV) | 5.066 |
| Betatron Tune $\nu_x/\nu_y$ | 59.283/45.102 |
| Chromaticity $\xi_x/\xi_y$ | −74.629/−59.628 |
| Momentum compaction $\alpha_p$ | 0.001426 |
| Rms dispersion $D_{\rm rms}$ (m) | 0.2132 |
| Maximum dispersion (m) | 0.6129 |
| Maximum betatron fcn $(\beta_x)_{\rm max}/(\beta_y)_{\rm max}$ (m) | 41.56/42.10 |
| Revolution frequency $f_0$ (kHz) | 49.034 |
| Revolution period $T_0$ ($\mu$s) | 20.394 |
| **RF System** | |
| RF frequency $f_{\rm rf}$ (MHz) | 499.999998 |
| RF harmonic $h$ | 10197 |
| RF voltage (for 12 cells) $V_{\rm rf}$ (MV) | 31.2 |
| Synchrotron tune | 0.037 |
| Synchronous angle (degrees) | 14.2 |
| **Beam** | |
| Extracted rms normalized emittance $\epsilon_{xN}/\epsilon_{xN}$ ($10^{-6}\pi$ m) | 4.66/0.020 |
| Rms energy spread | 0.0015 |
| Number of trains $n_{tr}$ | 60 |
| Number of bunches per train $n_b/n_{tr}$ | 47 |
| Number per bunch $N_b$ | $2 \times 10^{10}$ |
| Bunch spacing $\tau_{\rm sep}$ (ns) | 6.0 |
| Train separation for 59 trains/last train (ns) | 340/334 |
| RMS beam radius $\sigma_x/\sigma_y$ ($\mu$m) | 334/6.60 |
| RMS bunch length $\sigma_\ell$ (mm) | 5.67 |
| **Radiation Damping** | |
| Energy loss per turn $U_0$ (MeV) | 7.656 |
| Damping times $\tau_x/\tau_y/\tau_E$ (ms) | 27.0/27.0/13.5 |

are of length 1.9 km, only about 11% of the whole ring. As a result, the rms dispersion should be about 0.03 m, an order of magnitude smaller than that of the Fermilab design. In addition the rms horizontal beam radius coming from the emittance is 174.9 $\mu$m because the betatron function is twice as big as the Fermilab design. The horizontal beam size is therefore dominated by emittance. This difference has an important bearing on the incoherent space-charge tune shift to be discussed below.

### 2.1.1 Incoherent Self-Field Tune Shift

The incoherent space-charge tune shift at the center of the beam is, for the vertical,

$$\Delta\nu_y = -\frac{N_b r_e R}{2\pi\gamma^3\sigma_y(\sigma_x+\sigma_y)\nu_y B} = -0.0380 \tag{2.3}$$

and $\Delta\nu_x = -0.00057$ for the horizontal. In above, $r_e = 2.8179 \times 10^{-15}$ m is the classical electron radius and $N_b = 2\times 10^{10}$ is the number of particles per bunch. The bunching factor,

$$B = \frac{\sqrt{2\pi}\sigma_z}{C} = 2.33 \times 10^{-6}\ , \tag{2.4}$$

has been used. Notice that Eq. (2.3) gives the maximum vertical space-charge tune shift for particles at the center of the bunch. The vertical space-charge tune shift averaged over all particles in the bunch will be much less.

Simulation performed on the TESLA dog-bone damping ring reveals that a maximum space-charge tune shift of $-0.1$ is tolerable. [1] The maximum vertical space-charge tune shift of the TESLA dog-bone damping ring is $\Delta\nu_y = -0.31$. (The TESLA Report gives $\Delta\nu_y = -0.23$ because it has been incorrectly assumed that the average betatron functions are the same horizontally and vertically.) There are two reasons why this tune shift is an order of magnitude larger than that of the Fermilab design. First, since the vertical betatron tune of the TESLA ring is $\nu_y = 44.18$, almost the same as the Fermilab design, the space-charge tune shift is essentially proportional to the square of circumference of the ring and the TESLA dog-bone is 2.78 times larger. Second, the horizontal beam size of the Fermilab ring has been enlarged by a factor of 3 because of the dispersion, but this enlargement is almost negligible in the TESLA ring. In the analysis of Decking and Brinkmann, [1] the maximum vertical space-charge tune shift can be reduced to $\Delta\nu_y = -0.035$ by initiating horizontal and vertical coupling at the long straight sections so that average vertical and horizontal emittances are equal to about one half the designed $\epsilon_{xN}$. No such consideration will be necessary for the Fermilab damping ring.

### 2.1.2 Space-Charge Impedances

Taking the vertical radius of the beam pipe as $b = 2$ cm, space-charge impedances experienced by the beam are

$$\frac{Z_0^{\parallel}}{n} = -j\frac{Z_0}{2\gamma^2}\left(\gamma_e + 2\ln\frac{b}{\sqrt{2}\sigma_y}\right) = -j0.031 \text{ m}\Omega \ ,$$
$$Z_1^{\perp} = -j\frac{Z_0 R}{\gamma^2}\left(\frac{1}{\sigma_y(\sigma_y+\sigma_x)} - \frac{1}{b^2}\right) = -j1.66 \text{ M}\Omega/\text{m} \ , \tag{2.5}$$

where $\gamma_e = 0.57722$ is Euler's constant.[‡] We see that the longitudinal space-charge impedance is small and will be within the microwave stability limit. The vertical space-charge impedance, on the other hand, is large and is larger in magnitude than the transverse wall-resistive impedance at the $(1-Q)$ line. However, it may help in increasing the threshold of transverse mode-mixing instability of the beam to be discussed below. [2] The space-charge impedances of the TESLA design are comparable.

## 2.2 Button BPM

We are using the BPM computation made in the NLC ZDR. The button BPM of the NLC damping ring is shown in the left plot of Fig. 1. For a set of four, the magnitude of the longitudinal impedance calculated using MAFIA is shown in the right plot. The first resonance is 14 $\Omega$ at 9.1 GHz with $Q \sim 300$, while the second resonance is 16 $\Omega$ at 12 GHz with $Q \sim 50$. The revolution frequency of the Fermilab damping ring is $f_0 = 49.0$ kHz. Thus these two resonances give $\mathcal{R}e\, Z_0^{\parallel}/n = 0.0754$ m$\Omega$ and 0.0653 m$\Omega$ at the respective resonant frequencies.

The impedance of a resonance at angular frequency $\omega_r$ can be written as

$$Z_0^{\parallel}(\omega) = \frac{R_s}{1+jQ\Delta} \ , \tag{2.6}$$

with

$$\Delta = \frac{\omega}{\omega_r} - \frac{\omega_r}{\omega} \ . \tag{2.7}$$

The reactive part is

$$\mathcal{I}m\, Z_0^{\parallel}(\omega) = \frac{-R_s Q\Delta}{1+Q^2\Delta^2} \ , \tag{2.8}$$

[‡]Euler's constant is defined as $\gamma_e = \lim_{m\to\infty}\left(1+\frac{1}{2}+\frac{1}{3}+\frac{1}{4}+\cdots+\frac{1}{m}-\ln m\right)$.

which exhibits a maximum at

$$\frac{1 - Q^2\Delta^2}{(1 + Q^2\Delta^2)^2} , \tag{2.9}$$

or

$$Q\Delta = \mp 1 . \tag{2.10}$$

The peak value of the reactive part is therefore

$$(\mathcal{I}m\, Z_0^{\parallel})_{\rm pk} = \pm\frac{R_s}{2} , \tag{2.11}$$

and the peak frequency is at

$$\frac{\omega}{\omega_r} = \sqrt{1 + \frac{1}{4Q^2}} \mp \frac{1}{2Q} . \tag{2.12}$$

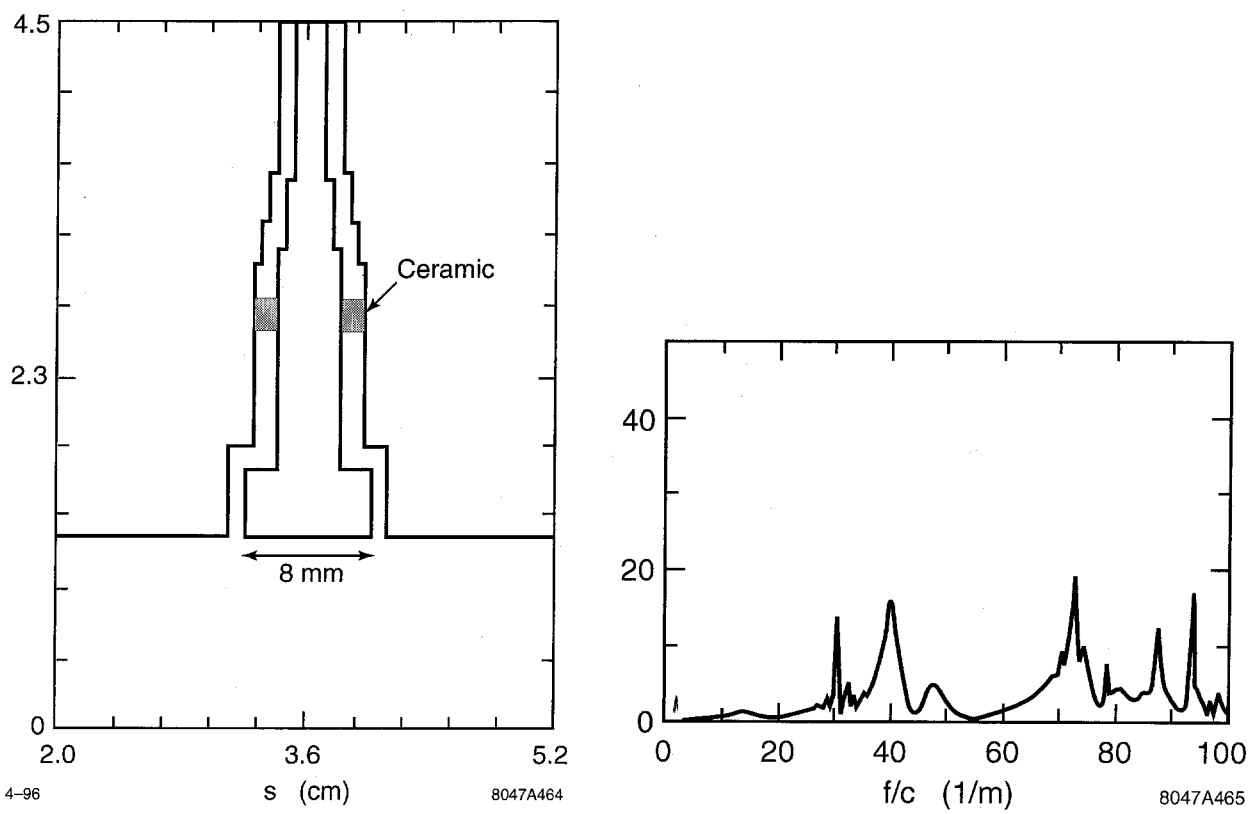


Figure 1: Left: Cross section of a NLC button BPM. Right: Magnitude of longitudinal impedance computed using MAFIA.

Thus for a high $Q$ resonance,

$$\frac{\mathcal{I}m\, Z_0^{\parallel}}{n} = \begin{cases} \frac{1}{2}\frac{R_s}{n_r} & \omega \sim \omega_r \\ \frac{1}{Q}\frac{R_s}{n_r} & \omega \ll \omega_r \ , \end{cases} \tag{2.13}$$

where $n_r = \omega_r/\omega_0$ and

$$\frac{\mathcal{R}e\, Z_0^{\parallel}}{n} = \begin{cases} \frac{R_s}{n_r} & \omega \sim \omega_r \\ \frac{nR_s}{n_r^2 Q^2} & \omega \ll \omega_r \ , \end{cases} \tag{2.14}$$

At low frequencies, the reactive impedance for a set of 4 buttons is $\mathcal{I}m\, Z_0^{\parallel}/n = 0.00156$ m$\Omega$ (0.00025 m$\Omega$ from the first resonance and 0.00131 m$\Omega$ from the second). On the other hand $\mathcal{I}m\, Z_0^{\parallel}/n = 0.0377$ m$\Omega$ and 0.0327 m$\Omega$ near the first two resonances.

If a set of BPM is installed at the end of each quadrupole, we need to count the total number of quadrupoles in the lattice of the Fermilab damping ring. In SEXTO, there are 11 ARC's each containing 4 quadrupoles, 2 SUPPRESSOR's each containing 8 quadrupoles, 20 STRCELL's each containing 4 quadrupoles, or a total of 99 quadrupoles (one in SUPPRESSOR is considered shared). In SEXT1, there are 11 ARC's each containing 4 quadrupoles, 2 SUPPRESSOR's each containing 8 quadrupoles, 15 STRCELL's each containing 2 quadrupoles, 2 STRWIG's each containing 4 quadrupoles, and 1 WIG containing 2 quadrupoles or a total of 99 quadrupoles (one is considered shared). The ring is made up of 4 SEXT0's and 2 SEXT1's. Thus there are 594 quadrupoles in total and there will be 594 sets of BPM's. In total, $\mathcal{R}e\, Z_0^{\parallel}/n = 44.8$ m$\Omega$ and 38.8 m$\Omega$ near the two resonances at 9.1 and 12.0 GHz. $\mathcal{I}m\, Z_0^{\parallel}/n$ will be half of those near the resonances and 0.93 m$\Omega$ at low frequencies.

As for energy loss, MAFIA gives $k_{\parallel} = 0.0203$ V/pC for each BPM set. But the NLC damping ring electron bunch length is $\sigma_\ell = 3.3$ mm while the Fermilab damping ring electron bunch length is $\sigma_\ell = 5.67$ mm. Assuming $\sigma_\ell^{-1/2}$ dependency the loss factor for all the BPM,s in the Fermilab ring will be 9.20 V/pC.

## 2.3 WALL IMPEDANCE

The beam pipe is made of aluminum with resistivity $\rho_s = 2.65 \times 10^{-8}$ Ω-m. The skin depth at revolution frequency is therefore

$$\delta_{s0} = \sqrt{\frac{2\rho_s}{\omega_0 \mu}} = \sqrt{\frac{2\rho_s R}{Z_0}} = 0.370 \text{ mm} . \tag{2.15}$$

Assuming a round beam pipe of radius $b = 2$ cm, the longitudinal and transverse impedances are

$$\begin{aligned} Z_0^{\parallel} &= (1+j)\frac{\rho_s R}{\delta_{s0} b}\sqrt{n} = (1+j)3.49 n^{1/2}\ \Omega , \\ Z_1^{\perp} &= \frac{2c}{b^2}\frac{Z_0^{\parallel}}{\omega} = (1+j)17.0|n-\nu_{x,y}|^{-1/2}\ \text{M}\Omega/\text{m} . \end{aligned} \tag{2.16}$$

The loss factor is the energy loss of the bunch if the total charge inside the bunch is one Coulomb. It can be written as

$$k_{\parallel} = \frac{1}{2\pi}\int_{-\infty}^{\infty} Z_0^{\parallel}(\omega) h(\omega) d\omega , \tag{2.17}$$

where $h(\omega)$ is the power spectrum of the bunch and is equal to, for a Gaussian linear distribution,

$$h(\omega) = e^{-\omega^2 \sigma_\tau^2} , \tag{2.18}$$

where $\sigma_\tau$ is the rms bunch length. For the resistive wall, we get

$$k_{\parallel} = \frac{\Gamma(\frac{3}{4})}{2\pi \omega_0^{1/2} \sigma_\tau^{3/2}} \mathcal{R}e\, Z_0^{\parallel}\Big|_{n=0} \tag{2.19}$$

or 14.9 V/pC.

## 2.4 RF System

The rf system of the Fermilab damping ring will be essentially the same as that of the TESLA damping ring, consisting of 12 superconducting Niobium 500-MHz cavities having total shunt impedance $R/Q = 45\ \Omega$ per cell and unloaded quality factor $Q_0 \approx 10^{10}$ at 2°K. Robinson's stability provides damping effect to the bunches at the fundamental resonance. The higher-order parasitic modes will be damped using dissipative material applied to the inner surface

of both beam pipes just outside the cryostat at room temperature. Experience at CESR and KEKB tells us that the quality factor of these modes can be reduced to a few hundred over the bandwidth 1–3 GHz. These modes will contribute $Z_0^{\|}/n = 2$ m$\Omega$ for the TESLA dog-bone damping ring together with a loss factor $k_{\|} = 8.8$ V/pC. The TESLA dog-bone damping ring has a circumference of 17 km and bunch length $\sigma_\ell = 6$ cm. For the Fermilab damping ring, they are scaled to $Z_0^{\|}/n = 5.7$ m$\Omega$ and $k_{\|} = 9.1$ V/pC. The contribution to low frequency inductive $Z_0^{\|}/n$ should be much less because of the large quality factors.

## 2.5 Summary

The TESLA Design Report assigns 17 m$\Omega$ to non-inductive part of $Z_0^{\|}/n$ for kickers and 11 m$\Omega$ to inductive part of $Z_0^{\|}/n$ for bellows and another 5 m$\Omega$ to inductive part of $Z_0^{\|}/n$ for "other components." We scale[§] them according to the size of the ring and obtain 48 m$\Omega$ for kickers, 11 m$\Omega$ for bellows, and 5 m$\Omega$ for others. In Table II we make a summary.

Table II: Longitudinal impedance per harmonic and loss factor for the Fermilab damping ring from various contributions.

| | | $Z_0^{\|}/n$ (m$\Omega$) | $k_{\|}$ (V/pC) |
|---|---|---|---|
| Non-inductive | RF cavities | 5.7 | 9.1 |
| | Resistive wall ($n = 0$) | 3.5 | 14.9 |
| | BPMs | 44.8 | 9.2 |
| | Kickers | $\sim 48$ | $\sim 40$ |
| | Total | $\sim 102$ | |
| Inductive | Bellows | $\sim 11$ | $\sim 1.3$ |
| | BPMs | 44.8 | |
| | Others | $\sim 5$ | $\sim 0.6$ |
| | Total | $\sim 60.8$ | |
| | Total loss factor | | $\sim 75.1$ |

[§]The number of bellows increases as the ring size and we assume the same for "other components".

# 3 SINGLE BUNCH INSTABILITIES

## 3.1 Microwave Instability

For a short bunch, the longitudinal instability is caused by the mixing of azimuthal modes 1 and 2. The stability limit is given by

$$\left.\frac{Z_0^{\parallel}}{n}\right|_{\text{eff}} = \frac{2\pi\alpha_p E}{eI_{\text{pk}}}\left(\frac{\sigma_E}{E}\right)^2 , \tag{3.20}$$

where $\alpha_p$ is the momentum compaction factor, $I_{\text{pk}}$ is the peak current, and

$$\left.\frac{Z_0^{\parallel}}{n}\right|_{\text{eff}} = \frac{\displaystyle\int_{-\infty}^{\infty} \frac{Z_0^{\parallel}(\omega)}{n} h(\omega)d\omega}{\displaystyle\int_{-\infty}^{\infty} h(\omega)d\omega} \tag{3.21}$$

is the impedance weighted over the power spectrum $h(\omega)$ of the bunch mode under consideration.

For a damping ring, this instability must be avoided. If not, the bunch length will grow when the bunch becomes unstable. When saturated, the instability stops and the bunch length will be shortened by radiation damping to a value that the instability starts again. This oscillation of bunch length, called saw-tooth instability, has been observed at the SLAC SLC damping ring and the Argonne APS. Since radiation loss changes with bunch length, so is the synchronous phase for rf compensation. As the bunch blew up, the higher-order losses decreased and the beam phase shifted by about $\frac{1}{2}^\circ$ at the 714-MHz rf cavity of the SLC damping ring. This translated into a $2^\circ$ jump at the S-band in the linac. This magnitude of phase error caused a problem with the rf bunch-length compressor in the ring-to-linac beam line. When this instability took place, the bunch would be incorrectly launched into the linac and might eventually be lost on the downstream collimators, causing the linac to trip the machine protection circuits.

For the Fermilab damping ring, this stability limit is $Z_0^{\parallel}/n\Big|_{\text{eff}} = 163$ m$\Omega$. The rms bunch length is $\sigma_\tau = \sigma_\ell/c = 18.9$ ps and total bunch length is assumed to be $\tau_L \sim 4\sigma_\tau = 75.7$ ps. The power spectra of azimuthal modes 1 and 2 peak at $f_1 \sim 2/(2\tau_L) = 13.2$ GHz and $f_2 \sim 3/(2\tau_L) = 19.8$ GHz having half width $\sim 6.6$ GHz. They are much above the beam pipe cutoff frequency $f_c \sim 5.7$ GHz (assuming beam pipe radius $b = 2$ cm), where the

coupling impedance starts rolling off. Apparently, we do not have that amount of impedance to drive this instability.

For the TESLA damping ring, the stability criterion of Eq. (3.20) gives a comparable stability limit. Since the momentum compaction and the fractional energy spread are slightly smaller, ($\alpha_p = 1.20 \times 10^{-4}$ versus $1.43 \times 10^{-4}$, $\sigma_E/E = 1.30 \times 10^{-3}$ versus $1.51 \times 10^{-3}$), the TESLA stability limit becomes $Z_0^{\parallel}/n|_{\text{eff}} = 100$ m$\Omega$.

As for the NLC damping ring, based on ZDR data: $\alpha_p = 0.000465$, $\sigma_E/E = 0.00090$, $\sigma_\ell = 3.9$ mm, $E = 1.98$ GeV, $N = 1.57 \times 10^{10}$ per bunch, the stability limit is $Z_0^{\parallel}/n|_{\text{eff}} =$ 61 m$\Omega$.

## 3.2 Transverse Mode-Coupling Instability

Transverse mode-coupling instability, sometimes known as strong head-tail is one of the cleanest instabilities to observe in all electron storage rings. The rigid dipole mode or azimuthal $m = 0$ mode shifts downwards with beam intensity, a general behavior for short bunches. On the other hand, the azimuthal $m = -1$ mode is not much affected. When the beam intensity is high enough, mode $m = 0$ meets mode $m = -1$ and an instability occurs. The threshold is roughly given by the shifting of mode $m = 0$ by the synchrotron frequency and can be represented roughly by

$$\frac{eI_b c\, Z_1^{\perp}\big|_{\text{eff}}}{2E\nu_y\omega_0\tau_L} \approx \nu_s\omega_0 \ , \tag{3.22}$$

or

$$Z_1^{\perp}\big|_{\text{eff}} \approx \frac{2E\nu_y\nu_s\omega_0^2\tau_L}{eI_b c} \ , \tag{3.23}$$

where

$$Z_1^{\perp}\big|_{\text{eff}} = \frac{\displaystyle\int_{-\infty}^{\infty} Z_1^{\perp}(\omega)h(\omega)d\omega}{\displaystyle\int_{-\infty}^{\infty} h(\omega)d\omega} \tag{3.24}$$

is the transverse impedance weighted over the longitudinal power spectrum $h(\omega)$ of the bunch mode under consideration. With total bunch length $\tau_L = 4\sigma_\ell/c$, we obtain the stability limit of $Z_1^{\perp}\big|_{\text{eff}} = 2.58$ M$\Omega$/m. Since the mixing is between modes $m = 0$ and $m = -1$, the frequency of the driving force should be of lower frequency than that driving the longitudinal mode-mixing instability, and is from 6.6 to 13.2 GHz. Unfortunately, estimation

of broadband transverse impedance has not been made for the ring. If we employ the Panofsky-Wenzel-like relation

$$Z_1^{\perp} = \frac{2c}{b^2}\frac{Z_0^{\parallel}}{\omega} , \tag{3.25}$$

we obtain the longitudinal-equivalent limit of $Z_0^{\parallel}/n|_{\text{eff}} = 530$ m$\Omega$. From the estimate made in Table II, it does not appear to have this sort of impedance to drive the instability. We may say that the beam in the Fermilab damping ring will be safe against transverse mode-mixing instability.

For the Fermilab damping ring, it is very possible that the transverse impedance is dominated by space charge. In addition, the incoherent space-charge tune shift is large and is of the same order of magnitude as the synchrotron tune. Under these circumstances, the threshold criterion of Eq. (3.22) may not be valid. This is because nonspace-charge transverse impedance shifts the $m = 0$ mode downward without much effect on the other modes. Instability occurs when the $m = 0$ mode meets the $m = -1$ mode. On the other hand, the transverse space-charge impedance shifts all modes downward except the $m = 0$ mode. Thus if the transverse space charge impedance is large enough, it will be much harder for the $m = 0$ and $m = -1$ modes to meet. In other words, the threshold of transverse mode-coupling instability will be pushed to a much higher current in the presence of strong space charge. An illustration from a *square-well air-bag model* [3] is shown in Fig. 2. The strong transverse space-charge impedance comes from the large circumference of the damping ring and the small transverse emittances of the beam. In short, we may say the beam in the Fermilab damping ring will be very safe against transverse mode-mixing instability.

For the TESLA dog-bone damping ring, the synchrotron tune $\nu_s$ scales with $R^{1/2}$ while the betatron tune is $\nu_y = 44.2$, very close to the 45.1 of the Fermilab ring. Equation. (3.23) suggests that the stability limit for the TESLA dog-bone damping ring scales with $R^{-1/2}$ or 1.80 M$\omega$/m. With the Panofsky-Wenzel-like relation, this translates to $Z_0^{\parallel}/n = 133$ m$\Omega$, which is large compared with the estimate of $|Z_0^{\parallel}/n| \approx 29$ m$\Omega$ of inductive and 25 m$\Omega$ non-inductive impedance for the vacuum chamber of the TESLA dog-bone ring. Again, the large incoherent space-charge tune shift, even after the reduction because of the initiation of horizontal-vertical coupling, should help in pushing the threshold current to a higher value. The transverse mode-coupling instability limit for the NLC damping ring is $Z_1^{\perp}|_{\text{eff}} \sim$ 0.50 M$\Omega$/m.

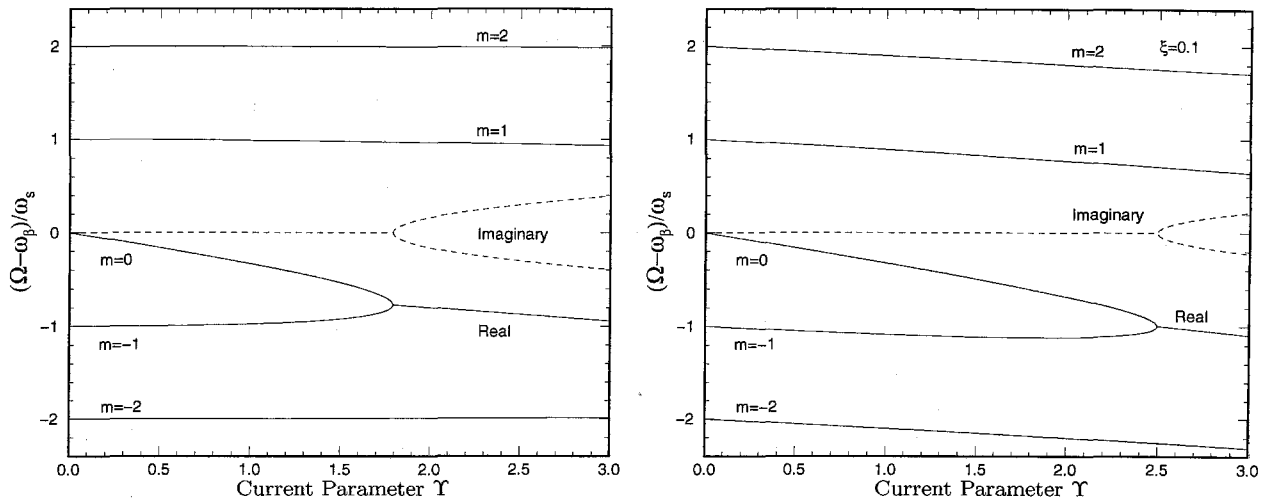


Figure 2: Illustration of space-charge effect on TMCI. Left: non-space-charge impedance drives the $m = 0$ mode downwards to meet with the $m = -1$ mode, while leaving all the other modes nearly unaffected at least at low intensity. Right: Space-charge force does not affect the $m = 0$ mode, but drives all other modes downwards. Thus the threshold at which the $m = 0$ and $m = -1$ modes meet will be pushed towards a high beam intensity. The current parameter $\Upsilon$ is the response of the tail particle in half a synchrotron period.

# 4 MULTI-BUNCH INSTABILITIES

## 4.1 Longitudinal Coupled-Bunch Instabilities

Each rf cavity has shunt impedance $R/Q = 45\ \Omega$. Assume the same for all the higher-order modes, which will be damped by dissipative material to $Q \sim 100$. Thus for all the 12 cavities, the largest possible shunt impedance for the higher-order modes will be $R_s = 54\ \mathrm{k}\Omega$. Assuming that this shunt impedance falls on a synchrotron sideband at about $\omega_r/(2\pi) = 1/(2\tau_L) \approx c/(4\sqrt{6}\sigma_z)3 = 5.4$ GHz, the frequency at which the bunch spectrum rolls off, the fastest longitudinal coupled-bunch growth rate given by

$$\frac{1}{\tau} = \frac{e\alpha_p n_b I_b R_s \omega_r}{4\pi E \nu_s} , \tag{4.26}$$

is only 49.1 $\mathrm{s}^{-1}$, where $I_b$ is the average bunch current, $n_b = 2820$ is the total number of bunches, and we have make use of the fact that the synchronous tune obtained from the bunch length and energy spread is

$$\nu_s = \frac{\alpha_p \sigma_E}{\sigma_\tau \omega_0 E} = 0.0370 . \tag{4.27}$$

Thus the shortest growth time is 36.6 ms. The above discussion assumes a ring filled with equally spaced bunches of *point* bunches of equal intensity. The finite length of the bunch will introduce a damping factor roughly equal to $\exp -(\omega_r^2 \sigma_\tau^2)$. The concentration of the bunches at 60 locations will further lower the growth rate. In short, the shortest growth time will be longer than the radiation damping time of 27 ms. Thus, no longitudinal coupled-bunch instability will materialize, and a broadband multibunch feedback system may not be necessary.

For the TESLA dog-bone ring, the shortest growth time is very much longer. The average bunch current $I_b$ scales with $R^{-1}$ while the synchrotron tunes $\nu_s$ scales with $R^{1/2}$, so that the shortest growth time scales with $R^{3/2}$ or 4.6 times longer. In addition, the momentum compaction $\alpha_p = 1.2 \times 10^{-4}$ is smaller than the Fermilab design and the rms bunch length $\sigma_\ell = 6$ mm is slightly longer. All these factors bring the shortest growth time for point bunches to 134 ms, about 4.7 damping times.

# 5 Transverse Coupled-Bunch Instabilities

The transverse resistive wall impedance will drive transverse coupled-bunch instabilities, and the fastest growing mode is driven by the vertical $(1-Q)$ betatron line. The growth rate is

$$\frac{1}{\tau} = \frac{e n_b I_b c}{4\pi \nu_y E} \mathcal{R}e\, Z_1^\perp F' \,, \tag{5.28}$$

where $F' \sim 0.8$ is a form factor depending on the longitudinal linear distribution. Although the betatron tune is $\nu_y = 45.1$, let us assume a residual tune of 0.5. The transverse wall impedance at the $(1-Q)$ line is $\mathcal{R}e\, Z_1^\perp = 24.0$ M$\Omega$/m and the growth rate is 1109.30 s$^{-1}$ (growth time 0.90 ms or 44 turns). We want to compare this growth rate with the TESLA dog-bone damping ring. The longitudinal resistive-wall impedance $Z_0^\parallel$ scales with $R^{1/2}$ because the skin depth at revolution harmonic scales with $R^{1/2}$. Thus the transverse resistive-wall impedance $Z_1^\perp$ scales with $R^{3/2}$ because it is proportional to $Z_0^\parallel/n$. The average bunch current will be smaller and scales with $R^{-1}$. Thus $I_b\, \mathcal{R}e\, Z_1^\perp$ and therefore the growth rate scales with $R^{1/2}$, since the vertical betatron tune of the TESLA ring is 44.18, very close to that of the Fermilab design. Thus the transverse coupled-bunch instability growth rate of the TESLA dog-bone ring will be $\tau^{-1} = 1910$ s$^{-1}$.

Due to the short bunch length, a shift towards positive chromaticity does not help at all.

This is because it requires a chromaticity $\xi_y \approx \alpha_p/(2f_0\tau_L) = 192$ to shift the mode spectrum of the bunch by $\Delta\omega = \pi/\tau_L$. The growth rate, however, can further be decreased by coating the beam pipe with a thin layer of copper. Tune spread supplied by octupoles can provide some amount of Landau damping. The remaining instability can be alleviated easily with a low-bandwidth feedback mode damper. The damper power required should be rather weak, because we only need to damp in 44 turns and the rigidity of the beam at 5.066 GeV is quite low, when compared with the former Fermilab Main Ring which stored the beam up to 150 GeV.

# 6 ELECTRON CLOUDS AND TRAPPED IONS

## 6.1 Electron-Cloud Effect

Electrons will be generated in the vacuum chamber of the damping ring due to residual gas ionization and secondary emission of residual gas ions or molecules hitting the wall of the vacuum chamber. In the positron ring, electron cloud will interact with the positron beam leading to a growth in transverse emittances. This interaction is short-range and the driving force can be represented by a short-range transverse wake $W_1$ left one bunch spacing ahead. [4] This wake computed for PEP-II gives $W_1 \lesssim 1 \times 10^5$ m$^{-2}$ in cgs units. Translating into MKS units, this becomes $W_1 \lesssim 890 \times 10^{12}$ V/Coul/m. The amplitude of transverse oscillation has a growth rate of

$$\frac{1}{\tau} \approx \frac{eI_bRW_1}{\nu_y E} , \tag{6.29}$$

or 301 s$^{-1}$ or a growth time of 3.33 ms. However, the amount of electron clouds can be greatly reduced by wrapping the beam pipe with solenoid. For example, simulation of the HER of KEKB shows that the transverse wake coming from electron cloud is $W_1 \lesssim 300$ m$^{-2}$, [5] which brings the growth rate to 1.11 s$^{-1}$ or a growth time of 901 ms, which is much longer than the radiation damping time of 27 ms. In fact, the whole beam will be stored and damped in the damping ring for about 0.2 s only. For the TESLA dog-bone ring, this growth rate will be relatively the same because $I_bR$ does not depend on the size of the ring and the vertical betatron tune is comparable to that of the Fermilab design.

## 6.2 Trapped Ions

Ions are generated in the vacuum chamber from the residual gas and the electron beam traps positively-charged ions. In the potential well of the electron beam, the trapped ions perform transverse oscillations with the ion-bounce angular frequencies

$$\omega_{ix,y} = \sqrt{\frac{3N_b r_p c}{\sigma_{x,y}(\sigma_x + \sigma_y)A\tau_{\text{sep}}}}\,, \tag{6.30}$$

where $r_p = 1.5347 \times 10^{-18}$ m is the classical proton radius, $A$ is the molecular weight of the ion, and $\tau_{\text{sep}}$ is the bunch separation. This expression is obtained by averaging over the whole train the individual kicks transferred to the ion from the point electron bunches. The ions will be cleared at the bunch gaps of length $\tau_{\text{sep}}$ if $\omega_{ix,y}\tau_{\text{sep}} > 2$, otherwise they will be trapped. For $CO^+$ with $A = 28$, the ion-bounce angular frequencies are $\omega_{ix} = 31.0$ MHz and $\omega_{iy} = 220$ MHz. We obtain $\omega_{ix,y}\tau_{\text{sep}} = 0.186$ and 1.32. Thus $CO^+$ will be trapped. For light ions such as $H_2^+$ with $A = 2$, $\omega_{ix,y}\tau_{\text{sep}} = 0.696$ and 4.96. Thus $H_2^+$ will be trapped horizontally but not vertically. On the other hand, bunch spacing is $\tau_{\text{sep}} = 20$ ns in the TESLA dog-bone ring, very much longer. As a result, $\omega_{ix,y}\tau_{\text{sep}} = 0.635$ and 2.51 for $CO^+$ and 2.37 and 9.40 for $H_2^+$. Thus only $CO^+$ will be trapped horizontally.

While the ions oscillate inside the electron beam, the electrons also oscillate inside the ion 'beam'. In the absence of external transverse focusing, small-amplitude electron-in-ion bounce angular frequency is

$$\omega_{ex,y} = \sqrt{\frac{4\lambda_i r_e c^2}{\gamma\sigma_{x,y}(\sigma_x + \sigma_y)}}\,, \tag{6.31}$$

where $\lambda_i$ is ion linear density. Compared with the ion-bounce frequency in Eq. (6.30), there is the extra $\gamma$ in the denominator because the electrons travel around the ring, and there is an extra factor of 2 in the numerator because the ions are at rest when generated by the electron, implying that the transverse radii of the ion 'beam' are a factor $\sqrt{2}$ smaller. The growth time in the linear theory can be expressed as

$$\tau_{x,y} = \frac{2\omega_{x,y}}{\omega_{ex,y}^2\omega_{ix,y}\tau_{tr}}\,, \tag{6.32}$$

where $\tau_{tr}$ is the length of the bunch train. Plugging in numbers gives $\tau_{x,y} = 360$ and 0.76 ms. Thus there is no worry in the horizontal direction, but some feedback device is necessary for the vertical. The results, together those for the TESLA dog-bone ring are listed in Table III. However, it is unclear why the growth times for the TESLA dog-bone are so

Table III: Possible fast-ion instabilities for trapped ions in the Fermilab damping ring and TESLA dog-bone ring at the vacuum pressure for $10^{-10}$ Torr.

| | Fermi | Dog-bone |
|---|---|---|
| Bunch spacing $\tau_{\rm sep}$ (ns) | 6 | 20 |
| For $H_2^+$ | | |
| Test for trapping $\omega_{ix}\tau_{\rm sep}$ | 0.70 | 2.37 |
| $\omega_{iy}\tau_{\rm sep}$ | 4.96 | 9.40 |
| For $CO^+$ | | |
| Test for trapping $\omega_{ix}\tau_{\rm sep}$ | 0.19 | 0.64 |
| $\omega_{iy}\tau_{\rm sep}$ | 1.32 | 2.51 |
| Linear Theory for $CO^+$ | | |
| Fast-ion growth time $\tau_x$ (ms) | 360 | 0.133 |
| $\tau_y$ (ms) | 0.76 | 0.002 |

much shorter than those for the Fermilab damping ring, although the trapping test shows that $CO^+$ will not be trapped in the former at least vertically. It is also unclear why the horizontal growth times are so much larger than the vertical ones, although the trapping test shows that trapping will be less severe in the horizontal. In fact, the expression of the growth time in Eq. (6.32) assumes a uniform electron beam of the length of the whole train without gaps so that ions are trapped inside.

In order to study the more realistic problem, some simulations have been performed. To save time on computation, only the first 1000 turns were simulated (total storage requires about 10000 turns). The vacuum pressure was increased to $10^{-8}$ to enhance the growth. All the bunches were considered as points and with a transverse offset randomly up to 1/100 of the rms radius. The vertical oscillation amplitudes for bunch 20 (left) and bunch 47 (right) in a train as picked up by a BPM is shown in Fig. 3 for the first 1000 turns. Since the vertical rms beam radius is $\sigma_y = 6.6 \times 10^{-6}$ m, the initial beam displacement was randomly between $\pm 6.6 \times 10^{-8}$ m. We see in the same figure that the growths in amplitude are very rapid reaching $\pm 8 \times 10^{-4}$ m already in 1000 turns for bunch 20 and $\pm 2.5 \times 10^{-4}$ m for bunch 47 and appear to continue. A feedback with a gain of 0.2 was then applied and the simulation repeated. We see that with feedback the amplitudes have been controlled to within $\pm 150 \times 10^{-6}$ m for bunch 20 and $\pm 25 \times 10^{-6}$ m for bunch 47. However, the oscillation amplitude for bunch 20 is still very much larger than the rms bunch radius. It is unclear why

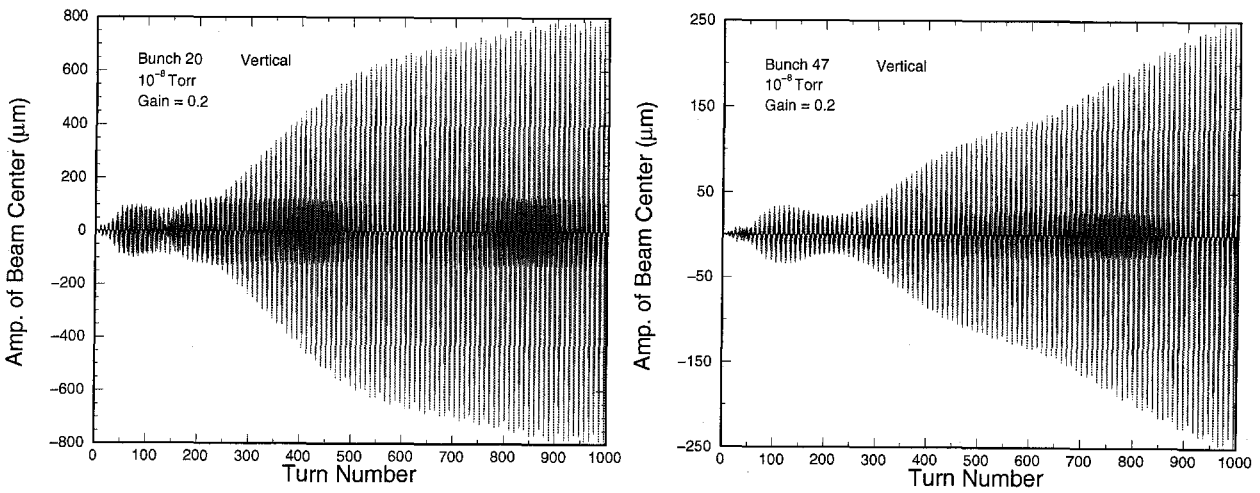


Figure 3: (color) Vertical amplitudes of the 20th bunch (left) and the 47th bunch (right) in the train for the first 1000 turns at vacuum pressure $10^{-8}$ Torr without and with feedback of gain 0.2. The growths have been very fast, but it was controlled by the feedback.

the growth of the last bunch of the train has been much less rapid than the 20th. The theory of fast beam-ion instability and some simulations [6] suggest that the instability growth rate increases with the square of the bunch position. On the other hand, we find in this train of 47 bunches that the bunches in the center of the train have much larger growths than the head and the tail bunches.

We repeat the simulations with vacuum pressure at $1\times^{-10}$ Torr. The results for bunches 20 and 47 are shown in the left and right plots of Fig. 4 Now the growth has been very much less in the first 1000 turns and went up to $\pm 15 \times 10^{-6}$ m for bunch 20 and $\pm 2.3 \times 10^{-6}$ m for bunch 47. Feedback of gain 0.20 stabilizes the growth to within $\pm 1.5 \times 10^{-6}$ m for bunch 20 and $\pm 0.4 \times 10^{-6}$ m for bunch 47, which are within the one sigma vertical half size of the beam.

In the horizontal direction, only the contribution from emittance has been used, which gives the horizontal radius of 87.8 $\mu$m. Thus the initial horizontal offset of the centers of the bunches have been offset randomly up to $\pm 0.88$ $\mu$m. The amplitudes of oscillation of the bunches are followed for the first 1000 turns. The results for bunch 20 are shown for vacuum pressure $1 \times 10^{-8}$ Torr in the left plot of Fig. 5 and for vacuum pressure $1 \times 10^{-10}$ Torr in the right plot. Here we see the amplitude grows to only $\pm 50 \times 10^{-6}$ m in the first 1000 turns at the vacuum pressure of $1 \times 10^{-8}$ Torr. With feedback of gain 0.2, the amplitude is damped to almost zero in 100 turns. At the vacuum pressure of $1 \times 10^{-10}$ Torr, there is no growth

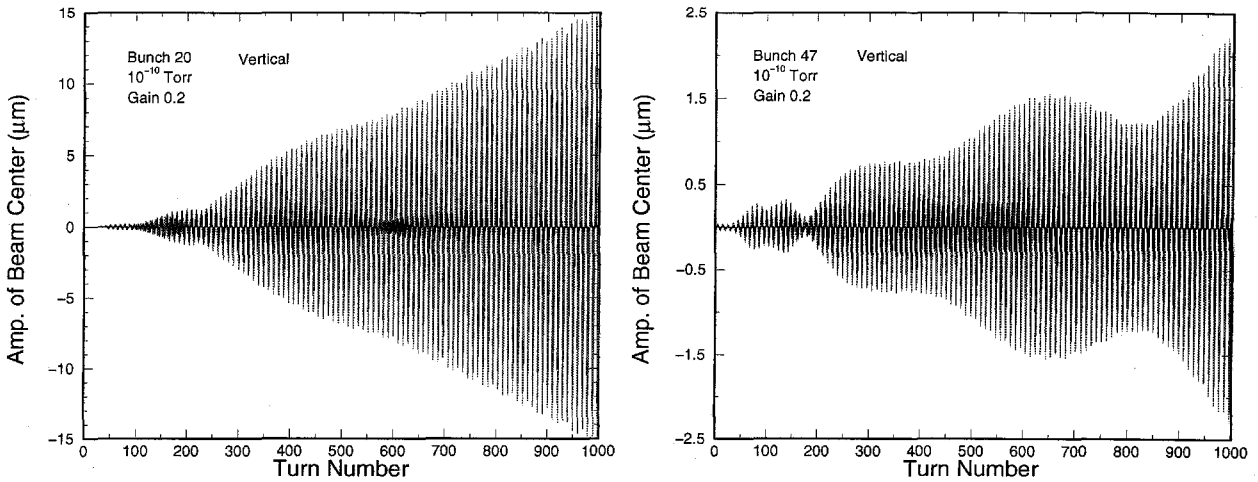


Figure 4: (color) Vertical amplitudes of the 20th bunch (left) and the 47th bunch (right) in the train for the first 1000 turns at vacuum pressure $10^{-10}$ Torr without and with feedback of gain 0.2. The growths have been much slower than when the pressure was $10^{-8}$ Torr. Feedback with a gain of 0.2 controls the oscillation of the bunch centers to within the rms size of the bunches.

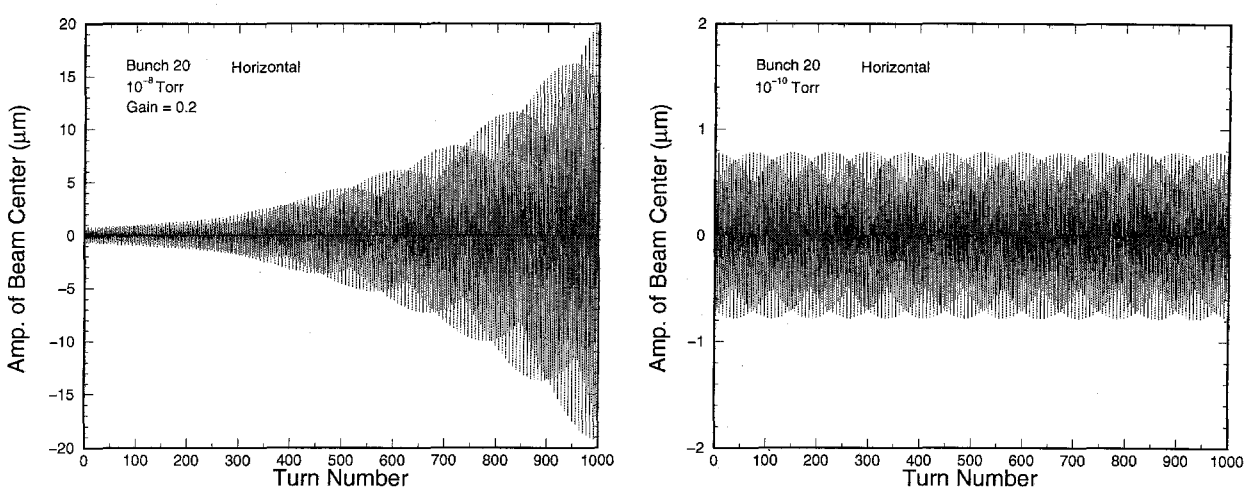


Figure 5: (color) Horizontal amplitudes of the 20th bunch in the train for the first 1000 turns at vacuum pressure $10^{-8}$ Torr (left) vacuum pressure $10^{-10}$ Torr (right). We see the amplitude grows when the pressure is $10^{-8}$ Torr and is damped to almost zero with feedback of gain 0.2. At vacuum pressure of $10^{-10}$ Torr, the bunch oscillation is stabilized without feedback.

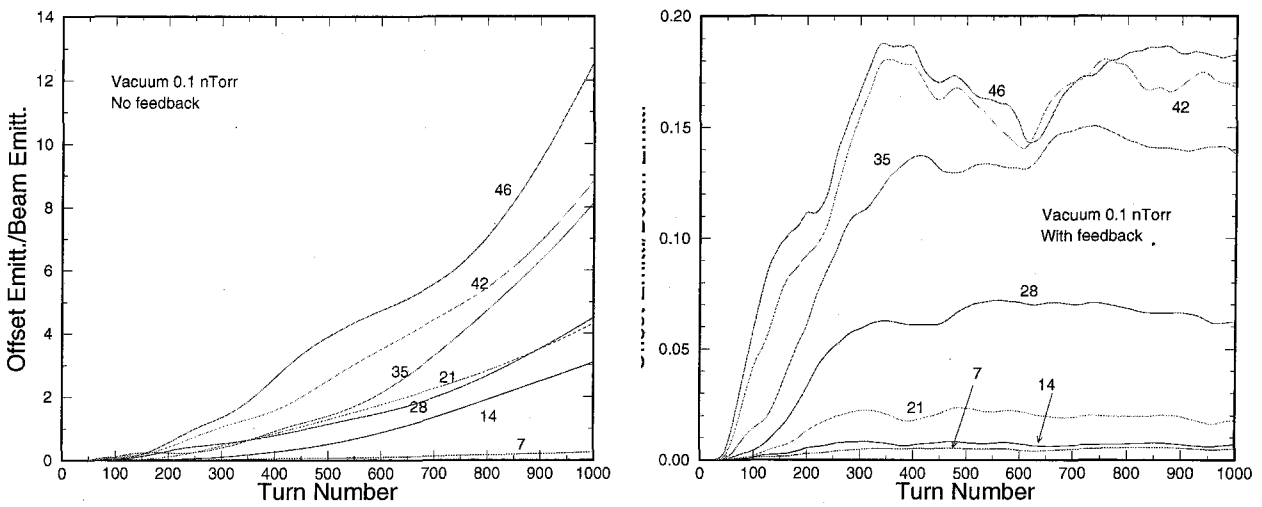


Figure 6: (color) Normalized offset emittance of bunches 7, 14, 21, 28, 35, 42, and 46. averaged over the 60 trains without/with feedback (left/right) at vacuum pressure of 0.1 nTorr. It is evident that the growth without feedback increases with bunch position. With feedback of gain 0.20, the offset emittance is controlled to within 20% of the vertical emittance of the beam.

at all, the beam just oscillates with the same amplitude of 0.88 $\mu$m.

So far we have been looking at only two bunches in a particle train. In order to have better statistics, we make averages over all the 60 trains. For this we define the offset emittance

$$\epsilon_{\text{offset}} = \frac{y^2_{\text{beamcenter}}}{\beta_y} , \tag{6.33}$$

and normalized it with respect to the vertical emittance of the beam. The averages of this normalized offset emittance over the 60 trains are shown in Fig. 6. The left plot is for bunches 7, 14, 21, 28, 35, 42, and 46 at vacuum pressure of 0.1 nTorr, and the right plot shows the same but with feedback of gain 0.20 turned on. We do find that the growth without feedback increases with bunch position, but it does not scale with the square of bunch position as postulated in Ref. [5]. With feedback turned on, the offset emittance is damped to within 20% of the beam vertical emittance. Or the vertical offset is within 10% of the vertical beam size. Notice that in these simulations, radiation damping has not been included. The radiation damping time is approximately 1400 turns. Thus when radiation damping is considered, the offset emittance will be much less. The amplitudes of oscillation of the bunches are simulated to be recorded at a beam-position motion but at different time. Now let us look at the motion of all the 2820 bunches altogether at a snapshot. To convert to bunch amplitudes at a snap-shot, the BPM values for the $j$th bunch in the $k$th train

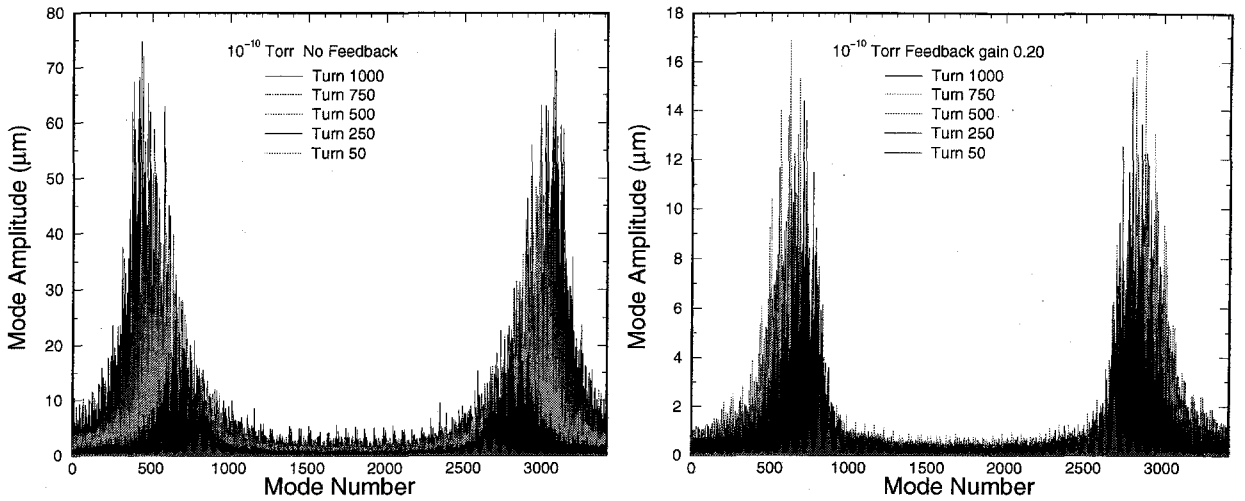


Figure 7: (color) Snapshot mode spectra are shown for the 50th, 250th, 500th, 750th and 1000th turns at vacuum pressure $10^{-10}$ Torr without and with (left and right) feedback of gain 0.2. The resonant modes correspond to $\ell = \nu_y + Q_{iy}$ and $(\nu_y - Q_{iy}) + N_{\rm sp}$. Without feedback the resonant amplitudes increase in time and the ion-bounce frequency decreases indicating that that the beam size increases. With feedback, both the resonant amplitudes and ion-bounce frequency reach saturation.

must be multiplied by the betatron phase $\exp\{i2\pi[57(k-1)+(j-1)]\nu_y/N_{\rm sp}\}$, where in the simulation we have assumed for simplicity 60 trains each containing 47 bunches followed by 10 empty bunch spacing and $N_{\rm sp} = 60 \times 57 = 3420$ is the total number of bunch spacings around the ring.

Fourier transform is made for each turn by multiplying the snapshot amplitude by ¶ $\exp[-i2\pi\ell m/N_{\rm sp}]$ and sum over the bunch spacing $m$ from 0 to $N_{\rm sp}-1$. The results in the vertical at the 50th, 250th, 500th, 750th and 100th turns are shown in Fig. 7 without and with (left and right) feedback of gain 0.20. According to the analysis of Chao [7], the resonant modes occur at $\ell = \nu_y - Q_{iy}$ where $\omega_{iy} = Q_{iy}\omega_0$ is the angular ion bounce frequency. Because the imaginary part of the amplitude is not monitored at the BPM, the Fourier transform results in another mirror resonance at $\ell = (\nu_y - Q_{iy}) + N_{\rm sp}$. These two resonances do appear for each snapshot in Fig. 7, and their mode number add up to $\approx 3510$, which is exactly $N_{\rm sp} + 2\nu_y$ as expected ($\nu_y = 45.1$). We identify the left resonant at $\nu_y + Q_{iy}$ and the right at $(\nu_y - Q_{iy}) + N_{\rm sp}$. Since they correspond to 815 and 2895 at the 50th turn, we obtain

¶If we multiply by $\exp[+i2\pi\ell m/N_{\rm sp}]$ instead, the two resonant modes in the mode spectrum will be at $\ell = Q_{iy} - \nu_y$ and $N_{\rm sp} - (\nu_y + Q_{iy})$. Note that the two resonances in the Fourier transform correspond to the same mode.

$Q_{iy} = 775$, which agrees very well with $Q_{iy} = 716$ using Eq. (6.30). Without feedback, as time goes on, the resonances shift to lower frequencies while their amplitudes become larger. This just reflects the evolution of the resonant beam-ion coupled oscillation with the beam size becoming larger and larger. With feedback turned on, we see that the $Q_{iy}$ does not increase any more after 250 turns and so are the resonant amplitudes. This reflects that an equilibrium has been reached in the presence of feedback, so that both the beam size and the oscillation amplitude do not increase anymore.

# 7 CONCLUSION

1. The reduced size of the Fermilab damping ring increases the rms dispersion of the ring by one order of magnitude compared to the TESLA dog-bone ring, so that the horizontal beam size becomes dispersion dominated. The reduction in ring size and the increase in horizontal beam size leads to a low tolerable coherent space-charge impedance. There is no need to resort to the method of vertical and horizontal coupling required in the TESLA damping ring

2. Longitudinal and transverse saw-tooth instabilities will be safe because the ring is below single bunch microwave instability limit and the transverse mode-coupling instability limit. Although the TESLA damping is also safe against these two instabilities, however, the threshold limits are lower.

3. Longitudinal coupled-bunch instability growth times driven by parasitic rf cavities higher order modes will be of the order of or longer than the radiation damping time. Those for the TESLA damping ring are longer. No damper will be necessary for both rings.

   Transverse coupled-bunch instability growth times driven by the resistive-wall impedance will be longer than 0.9 ms and a transverse narrowband mode damper will be necessary. Those for the TESLA damping ring are about twice longer and a transverse narrowband mode damper is also required.

4. Electron-cloud effect may be important. Like the KEKB HER ring, the effects can be avoided by wrapping the vacuum chamber with solenoids.

5. Fast beam-ion instability will occur. Simulation of the first 1000 turns show that the growth in amplitude can be alleviated with a feedback damping of gain 0.20.

# References


[1] W. Decking and R. Brinkmann, *Space Charge Problems in the TESLA Damping Ring*, Proc. 7th EPAC, Vienna 2000, p.1024.

[2] M. Blaskiewicz, *Fast Head-tail Instability with Space Charge*, Phys. Rev. ST Accel. Beams, **1**, 044201 (1998).

[3] V. Danilov and E. Perevedentsev, *Strong Head-Tail Effect and Decoupled Modes in the Space-Time Domain*, *Proceedings of XVth International Conference on High Energy Accelerators*, p.1163 (Hamburg, 1992);

[4] M.A. Furman and G.R. Lambertson, *The Electron-Cloud Instability in the PEP-II Positron Ring*, Proc. Int. Workshop on Multibunch Instabilities in Future Electron and Positron Accelerators (MBI'97), Tsukuba, KEK, 15-18 July, 1997, KEK Proceedings 97-17 1997, p.170.

[5] F. Zimmermann, *Accelerator Physics studies for KEKB: Electron Trapping, Electron Cloud in the HER, Closed-Orbit Drift, Horizontal Instability and Tune Shift*, KEKB Commissioning Report, April 2, 2002, and CERN SL-Note-2002-017 AP (2002).

[6] T.O. Raubenheimer and F. Zimmermann, A Fast Beam-Ion Instability in Linear Accelerators and Storage Rings, Phys. Rev. **E52**, 5487 (1995)

[7] A.W Chao, *Lecture Notes on Topics in Accelerator Physics*, US Particle Accelerator School at SUNY Stony Brook, New York, June 5-16, 2000.